

# Synthesis, Structure, and Physicochemical and Catalytic Characterization of the Novel High-Silica Large-Pore Zeolite SSZ-42

Cong-Yan Chen, Larry W. Finger, Ronald C. Medrud, Charles L. Kibby, Peter A. Crozier, Ignatius Y. Chan, Thomas V. Harris, Larry W. Beck, and Stacey I. Zones\*

**Abstract:** The novel high-silica zeolite SSZ-42 was synthesized and characterized by X-ray diffraction, scanning electron micrographs, transmission electron micrographs, argon and hydrocarbon adsorption, elemental analysis,  $^{13}\text{C}$  MAS NMR, FTIR, and catalytic reactions. The framework topology of SSZ-42 has been determined from X-ray diffraction data taken from a small

single crystal ( $15 \times 15 \times 35 \mu\text{m}$ ) and refined from powder diffraction data. The crystalline architecture is characterized by an undulating, one-dimensional 12-membered T-atom ring (12-MR) channel system. This configuration is a sur-

prise given that the measured adsorption capacity is much higher than expected for a one-dimensional channel system. The material is stable up to at least  $800^\circ\text{C}$  under thermal and hydrothermal conditions, and exhibits many interesting characteristics and promises to be a useful catalyst for hydrocarbon processing.

**Keywords:** structure elucidation • zeolite analogues • zeolites

## Introduction

The widespread use of zeolites as catalysts, adsorbents, and ion exchangers has had a remarkable impact on many industrial processes. The significant catalytic activity and selectivity of zeolite materials are attributed to the large internal surface area and highly distributed active sites that are accessible through uniformly sized pores. An important feature is that these pores are of the same molecular dimension as the reacting organic molecules. The use of organo-cation template molecules to provide structure direction has given rise to a number of novel high-silica zeolites in recent years, leading to breakthroughs in zeolite science and providing an impetus in developing new process chemistry.<sup>[1]</sup> As a consequence, the understanding of zeolite structures and the structure–property relationships has become not only of

basic academic interest but also one of the most critical tasks in bringing the industrial applications of these materials to successful fruition.

Typical hydrothermal conditions for zeolite synthesis usually do not yield sufficiently large crystals for the direct determination of the structure using single-crystal X-ray diffraction.<sup>[2]</sup> Several exciting new molecular sieve structures such as EU-1,<sup>[3]</sup> beta,<sup>[4]</sup> ZSM-18,<sup>[5]</sup> NU-87,<sup>[6]</sup> SSZ-26/SSZ-33,<sup>[7]</sup> MCM-22,<sup>[8]</sup> RUB-3,<sup>[9]</sup> UTD-1,<sup>[10]</sup> VPI-8,<sup>[11]</sup> VPI-9,<sup>[12]</sup> and SSZ-31<sup>[13]</sup> have been solved with a combination of several techniques, such as X-ray powder diffraction, high-resolution electron microscopy, electron diffraction,  $^{29}\text{Si}$  MAS NMR spectroscopy, and a knowledge of the material's porosity and its relationship to framework density. This information is combined with computational techniques to generate models, from which trial structures are then compared to experimental diffraction data by a Rietveld refinement. Clearly, synthesizing sufficiently large, high-quality crystals and developing suitable structure models remain a considerable but beneficial challenge.

In this paper we report the discovery, synthesis, crystalline structure, physicochemical and catalytic characterization of a novel zeolite designated as SSZ-42.<sup>[14, 15]</sup> This is the first reported solution of a high-silica large-pore zeolite structure based on single-crystal data. The outcome represents quite a surprise from the indications given by each of the individual techniques cited above (vide infra). These analytical tools hinted at a multidimensional pore system with at least one 10- and one 12-membered T-atom ring (12-MR), as has been observed for SSZ-33.<sup>[7]</sup>

[\*] Dr. S. I. Zones, Dr. C. Y. Chen, Dr. R. C. Medrud, Dr. C. L. Kibby, Dr. I. Y. Chan, Dr. T. V. Harris  
Chevron Research & Technology Co., Richmond, CA 94802 (USA)  
Fax: (+1) 510-242-1599  
E-mail: cych@chevron.com

Dr. L. W. Finger  
Carnegie Institution of Washington, Geophysical Laboratory,  
Washington, D. C. 20015 (USA)

Dr. P. A. Crozier  
Center for Solid State Science, Arizona State University,  
Tempe, AZ 85287 (USA)

Dr. L. W. Beck  
Chemical Engineering, California Institute of Technology,  
Pasadena, CA 91125 (USA)

## Experimental Section

**Synthesis:** The SSZ-42 materials were synthesized by using *N*-benzyl-1,4-diazabicyclo[2.2.2]octane cation,  $R^+$ , as the template molecule (see Table 1).<sup>[6]</sup> The borosilicate versions used here for the structure analysis were prepared with synthesis mixtures of composition  $0.150 R_2O:0.018 Na_2O:0.037 B_2O_3:SiO_2:43.3 H_2O$ . The synthesis procedure for the powder sample ( $\approx 1-2 \mu m$ ) is outlined as follows: An aqueous ROH solution (18.11 g,  $0.9 \text{ mol L}^{-1}$ ) was used to dissolve sodium tetraborate decahydrate (0.38 g) ( $Na_2B_4O_7 \cdot 10 H_2O$ , Aldrich) in  $H_2O$  (27.5 g). Then Cab-O-Sil M-5 silica (Cabot) (3.26 g) was stirred into the resulting solution. The reaction mixture was further stirred at room temperature for 1 hour. Finally the resulting synthesis gel was heated in a Teflon-lined stainless steel autoclave under static conditions at  $150^\circ C$  for 17 days. The solid products were recovered by filtration, washed with deionized water, and dried in air at room temperature.

In one batch we were fortunate to find single crystals of uniform size (ca.  $15 \times 15 \times 35 \mu m$ ). For this synthesis we used boric acid ( $H_3BO_3$ , Mallinckrodt) (0.25 g) and NaOH (EM Sciences) (0.08 g) as sources of boron and sodium, and the synthesis gel was heated under otherwise identical conditions for 10 days.

To remove the occluded template molecules, the as-synthesized powder sample was calcined in a steady stream of nitrogen containing just a slight bleed of air. The stages were as follows: first from room temperature to  $125^\circ C$  at  $50^\circ C h^{-1}$  and hold for two hours, then to  $540^\circ C$  at  $50^\circ C h^{-1}$  and hold for four hours, subsequently to  $600^\circ C$  at  $50^\circ C h^{-1}$  with a final hold for four hours.

The synthesis procedures of other zeolites used here for comparison studies in physisorption have been described in early works.

**X-ray diffraction:** To identify the crystallized phases and to test for phase purity, the X-ray powder diffraction patterns (for both powder and single-crystal samples) were collected by using  $Cu_{K\alpha}$  radiation on a in-house Siemens D500 diffractometer equipped with a graphite monochromator and scintillation detector.

To solve the framework arrangement of SSZ-42, single-crystal data for a sample containing the occluded template molecules were collected with a CCD camera in the Applications Laboratory of Siemens Energy and Automation, Inc. in Madison, Wisconsin, USA. This single crystal (ca.  $15 \times 15 \times 35 \mu m$ ), has a scattering power equal to about  $4 \times 10^{14}$ , which is nearly three orders of magnitude smaller than typical crystals used in the usual experiment with a laboratory, sealed source. This scattering power is defined as  $\rho^2 V_C \lambda^3$ , where  $\rho$  is the average electron density,  $V_C$  is the volume of the crystal, and  $\lambda$  is the wavelength of the experiment. Despite the small size of the crystal, and a data collection that was not particularly optimized for low scattering power, 50% of the observations to a resolution of  $1.0 \text{ \AA}$  have  $F^2 > 2\sigma(F^2)$ ; however, this crystal size is clearly close to the lower limit for this type of instrument. The data from this very small SSZ-42 crystal were sufficient to locate the framework atoms by using direct methods in SHELXTL (version 5.03)<sup>[17]</sup> to generate a very good trial model, but not precise enough to get good bond lengths and angles. The crystal system is monoclinic, and the diffraction pattern is consistent with space group  $C2/m$ . There are four topologically distinct T-atoms (T = tetrahedrally coordinated) and 10 O atoms.

To refine the SSZ-42 structure determined by the single-crystal analysis, full powder patterns for both calcined and as-synthesized powder samples (crystal size ca.  $1-2 \mu m$ ) were collected at high-resolution beamline X7A of the National Synchrotron Light Source (NSLS) with the samples sealed in a capillary and rotated about the capillary axis. The calcined sample used for the powder diffraction was prepared by heating the calcined material at  $350^\circ C$  for several hours in a glass capillary under vacuum, to remove as much of the adsorbed species as possible, and then sealing. The synchrotron radiation from the bending magnet source was monochromatized with a channel-cut Si 220 crystal, and the wavelength and diffractometer zero were calibrated with a standard silicon sample. The values of the wavelengths were  $1.15207$  and  $1.14833 \text{ \AA}$  for the calcined and as-synthesized samples, respectively. Maximal resolution was ensured by the use of a germanium 200 analyzer crystal.<sup>[18]</sup> Instrumental parameters were determined by using the structure-independent intensity extraction method of Le Bail et al.,<sup>[19]</sup> as suggested by Cox.<sup>[20]</sup> Fixed backgrounds were selected in the regions where no reflections occurred, and the asymmetric profile

function of Finger et al.,<sup>[21]</sup> which properly accounts for axial divergence, was employed by using the computer program GSAS.<sup>[22]</sup> Refined in this stage were two Lorentzian and one Gaussian profile parameters, two asymmetry parameters, the lattice constants, and the diffractometer zero. After convergence, the slope of the normal probability plot<sup>[23]</sup> was used as a multiplier for the estimated standard deviations of the measured data. In both cases, the esds of the count data had been underestimated by a factor of 1.3 to 2. In final convergence,  $\chi^2$  for the Le Bail fit was essentially unity for both samples. At this stage, the profile parameters were fixed and the structural refinement begun with the atomic positions determined from the direct methods solution. For both samples, the final cycle of refinement included the lattice constants, the profile coefficients, preferred orientation parameters,<sup>[24]</sup> and the structural parameters with isotropic temperature factors for all atoms. Backgrounds determined in the initial stage were fixed in the final refinement.

**Electron microscopy:** The scanning electron micrographs (SEM) were obtained on a Hitachi S-570 scanning electron microscope.

The initial electron diffraction and imaging analysis were conducted on a JEOL 100CX transmission electron microscope. Detailed high-resolution transmission electron microscopy (HREM) were performed on a JEOL 4000 EX transmission electron microscope operating at 400 kV with a point-to-point resolution of  $2.2 \text{ \AA}$  at Arizona State University. The specimens used in the HREM experiments were prepared by crushing the calcined SSZ-42 and dispersing the thin sections over a holey carbon film supported on a copper grid.

**Physisorption:** Argon physisorption measurements were made in an Omnisorp 100CX instrument from Coulter. Adsorption isotherms were measured at  $-186^\circ C$  by both static and continuous flow techniques, after the samples were degassed in vacuum ( $< 10^{-6}$  Torr) at  $300^\circ C$  for two hours. With continuous flow, about 1000 data points were obtained for argon pressures between  $10^{-6}$  and 550 Torr. Sample sizes were about 100 mg and the argon flow was slow enough that it took one to two hours to admit enough argon to fill the samples' micropores. With static adsorption, equilibration times were ten minutes for each data point. Doses were small enough that five to ten hours were required to admit enough argon to fill the micropores. Micropore volumes and external areas were estimated from alpha-plot analyses of the adsorption isotherms, using alpha values obtained from a silica standard (CPG-75).

The adsorption capacities of zeolites for vapor phase hydrocarbons were measured at room temperature using a Cahn C-2000 balance coupled with a computer through an ATI-Cahn digital interface.<sup>[25]</sup> The adsorbates studied were *n*-hexane, 2,2-dimethylbutane, cyclohexane, 1,2,4-, and 1,3,5-triisopropylbenzene. The vapor of the adsorbate was delivered from the liquid phase. The relative vapor pressure  $p/p_0$  was maintained at about 0.3 by controlling the temperature of the liquid adsorbate using a cooling circulator. Prior to the adsorption experiments, the calcined zeolites were dehydrated at about  $350^\circ C$  under a vacuum of  $10^{-3}$  Torr for 5 h. The adsorption capacities are reported in milliliters of liquid per gram of dry zeolite, under the assumption that the adsorbed adsorbate has the same density as the bulk liquid.

**Additional physicochemical characterization:** The elemental analyses were performed by Galbraith Laboratories (Knoxville, TN, USA).

Solid-state  $^1H$  NMR spectra of as-synthesized SSZ-42 powder sample were acquired at 7.0 T and 300 MHz. The Bruker 300 AM spectrometer was equipped with high power amplifiers and magic angle spinning (MAS) probes for high resolution.  $^{13}C$  MAS NMR spectra were acquired using the six-pulse version of the TOSS sequence to suppress spinning sidebands following the creation of coherent magnetization by cross-polarization (CP).<sup>[26]</sup> The sample spinning rate was 4.0 kHz, the cross-polarization time was 2 ms, the decoupling field strength was 60 kHz, and the recycle delay was 2 s.  $^{13}C$  MAS NMR spectra were also acquired after a brief period, 28.5 ms, with no  $^1H$ -decoupling. This dipolar-dephasing experiment was used to discriminate between mobile and rigid components of the NMR spectrum.<sup>[26, 27]</sup>

The IR spectra of zeolites were measured in a Nicolet Magna 550 FTIR spectrometer equipped with a KBr beamsplitter, a diamond ATR cell from ASI, and a DTGS detector. The ATR cell had a KRS-5 crystal that gave useful spectra down to  $350 \text{ cm}^{-1}$ .

**Catalysis:** The catalytic test reactions were conducted according to the procedures reported elsewhere.<sup>[16, 28-31]</sup>

## Results and Discussion

**Synthesis:** We synthesized SSZ-42 and recognized it as a new zeolite material several years ago while trying to solve a particular zeolite synthesis problem. We had had good success in synthesizing zeolite SSZ-16<sup>[32]</sup> using templates based upon linking 1-azabicyclo[2.2.2]octane units with a methylene chain, particularly with three to five methylene groups.<sup>[33]</sup> An improvement was the finding that the isostructural diazabicyclo[2.2.2]octane also works.<sup>[34]</sup> The latter is often characterized in the organic chemistry literature as DABCO and is available as a very large commodity chemical (used as a catalyst in the production of polyurethanes). In a given synthesis problem we also wanted to use the latter diquaternary ammonium compound (or template) to make Al-rich beta zeolite. But the SSZ-16 zeolite also began to form as an impurity in some reaction attempts, as the Al content increased in the synthesis gels. The two zeolites have very different structures (Figure 1) and catalytic properties. We

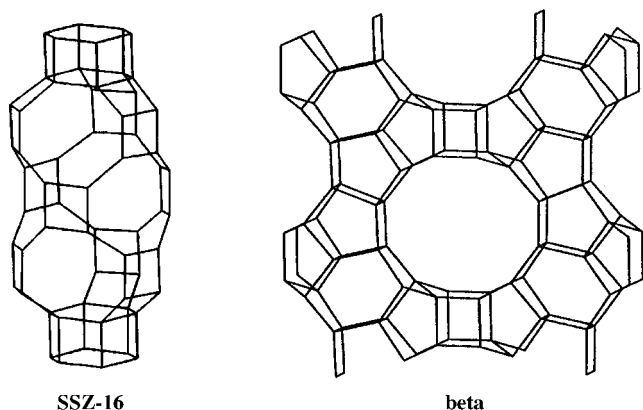
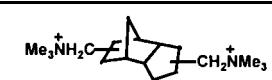
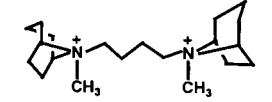
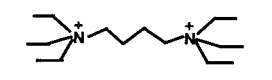
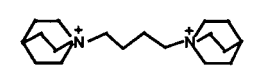
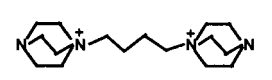
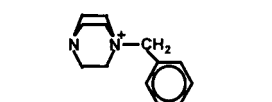
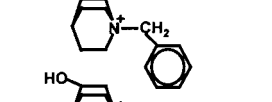
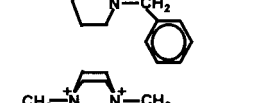
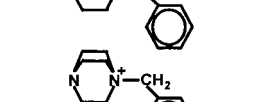
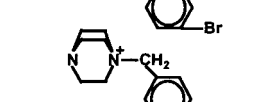
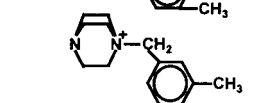
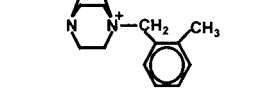
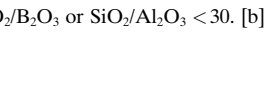


Figure 1. Crystalline structures of SSZ-16 and beta.

thought that a bent configuration, off the DABCO nitrogen center, would still allow us to form the multichannel beta zeolite but would eliminate the large cavity-dominated crystallization of SSZ-16. We chose to try a benzyl derivative, namely, *N*-benzyl-1,4-diazabicyclo[2.2.2]octane cation (Table 1, entry 6).

The strategy proved successful with the DABCO derivatives. As one moved to higher and higher  $\text{SiO}_2/\text{Al}_2\text{O}_3$  values in the synthesis gel, the beta zeolite was replaced by either mordenite or eventually ZSM-12 at the highest ranges. We recently described this change in product with changing lattice substitution for polycyclic template molecules with regard to both aluminosilicate and borosilicate systems.<sup>[35]</sup> The DABCO derivative described above for use in making both beta zeolite and SSZ-16 had also been found to be a particularly good template for preparing beta zeolite in its weakly acidic borosilicate form, removing any need for Al in the synthesis.<sup>[36]</sup> Thus the next question to consider was would this newer benzyl derivative also make beta zeolite as a borosilicate? The answer is that the novel SSZ-42 appeared instead.<sup>[16]</sup> While structurally different from beta zeolite, SSZ-42 also shows some indications as to why the two might be

Table 1. Organic templates and the resulting zeolites.

Entry	Organic template	Zeolite at high lattice substitution <sup>[a]</sup>	Zeolite at moderate lattice substitution <sup>[b]</sup>
1		SSZ-16 (Al)	–
2		SSZ-16 (Al)	–
3		SSZ-16 (Al)	MTW (Al)
4		SSZ-16 (Al)	MTW (Al)
5		SSZ-16/beta (Al)	MTW (Al)
6		beta (Al)/SSZ-42 (B)	SSZ-42 (B)
7		SSZ-42 (B)	SSZ-42 (B)
8		SSZ-42 (B)	SSZ-42 (B)
9		kenyaite	kenyaite
10		amorphous (B)	MTW (B)
11		amorphous (B)	MTW (B)
12		amorphous (B)	MTW (B)
13		amorphous (B)	MTW (B)

[a]  $\text{SiO}_2/\text{B}_2\text{O}_3$  or  $\text{SiO}_2/\text{Al}_2\text{O}_3 < 30$ . [b]  $\text{SiO}_2/\text{B}_2\text{O}_3$  or  $\text{SiO}_2/\text{Al}_2\text{O}_3 > 40$ .

grouped together as part of a family of structures resulting from similar synthesis chemistry.

Once the parameters for making the SSZ-42 as a borosilicate were well-defined, we moved on to looking at related template derivatives, many of which are shown in Table 1. The template proved to be quite spatially selective as we learned once the zeolite structure became known, as well as from the results of template synthesis studies. Thus, it appears that the various ring-substituted benzyl derivatives we were able to make (Table 1, entries 10–13) all increased the size too much in terms of a critical fit or packing sector of the zeolite. Most

of these derivatives made ZSM-12 instead, extending themselves down a linear channel. Using the isostructural quinuclidine for DABCO worked fine (Table 1, entry 7) and this latter template has been also successfully used to make the aluminosilicate zeolite MCM-58<sup>[37]</sup> and more recently the pure-silica zeolite ITQ-4.<sup>[38]</sup> According to the Structure Commission of the International Zeolite Association, these two zeolites are isostructural to SSZ-42. We also were successful with the quinuclidinol derivative (Table 1, entry 8). Thus, it appears that changes to the bicyclo[2.2.2]octane segment are less critical than derivatives of the benzyl substituent (vide infra for <sup>13</sup>C MAS NMR results).

**SEM and optical microscopy:** Figure 2 shows the morphologies and sizes of two as-synthesized SSZ-42 samples studied here. The sample shown in Figure 2a was made up of large single crystals of very uniform size (ca. 15 × 15 × 35 μm). No twinned crystals were observed in this sample. When examined under a high-resolution optical microscope, the single crystal extinguished uniformly under crossed polarizers, indicating they were truly single crystals. The orientation of the optic axes of these single crystals is consistent with the monoclinic symmetry determined from the X-ray diffraction data (vide infra). The sample shown in Figure 2b had a uniform crystal size of about 1–2 μm. As shown in Figure 3, the X-ray diffraction (XRD) patterns of both samples contained peaks characteristic of SSZ-42. The peak intensities of single-crystal SSZ-42 were affected by texture because the sample no longer had a random distribution of particles due to the large size of the crystal (15 × 15 × 35 μm).

**Details of structure:** The unit cell parameters of both as-synthesized and calcined samples are shown in Table 2. They were determined based on the full powder patterns (crystal size ca. 1–2 μm) collected at high-resolution beamline X7A of the National Synchrotron Light Source, Brookhaven National Laboratory. Calcination results in a contraction of the unit cell in *a* and *c* directions but expansion in the *b* direction. The resulting contraction of unit cell from 1851.12

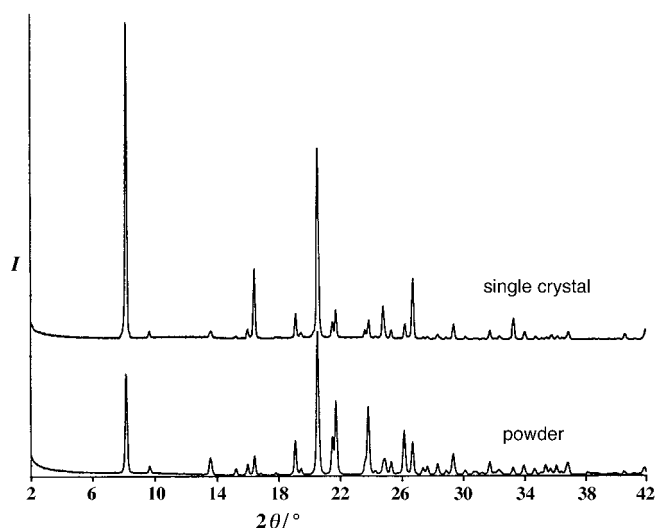


Figure 3. Conventional X-ray powder diffraction patterns of the two as-synthesized SSZ-42 samples described in Figure 2 (taken on in-house Siemens D500 diffractometer).

Table 2. Unit cell parameters for SSZ-42.

	<i>a</i> [Å]	<i>b</i> [Å]	<i>c</i> [Å]	β [°]	<i>V</i> [Å <sup>3</sup> ]
as-synthesized	18.6309(9)	13.3359(1)	7.61731(3)	102.017(1)	1851.12(1)
calcined	18.4991(2)	13.4078(1)	7.57548(2)	101.471(1)	1841.49(2)

to 1841.49 Å<sup>3</sup> implies, together with the relationships between template geometry and zeolite structure discussed above (see Table 1), that the template molecules are tightly packed in the channel system of SSZ-42, and the zeolite framework is relaxed upon removal of the occluded template molecules (vide infra for <sup>13</sup>C MAS NMR results).

For the refinement of the powder data from the calcined sample, which contains only the framework atoms, convergence was accomplished without difficulty by using the program GSAS. Difference electron density slices through the channel cross-section showed no residual electron density. The refinement led to residuals of  $wR_p = 0.066$ ,  $R_p = 0.050$ ,

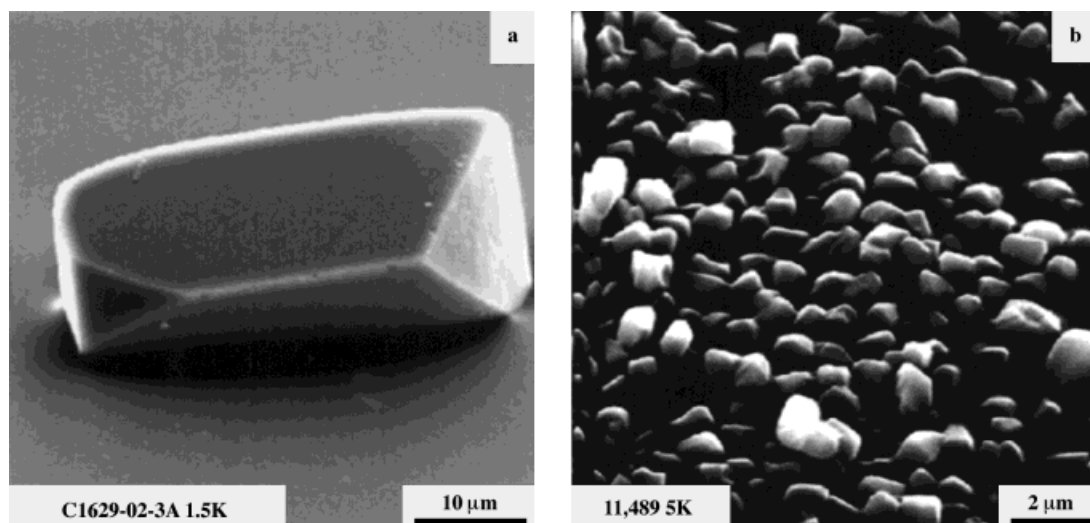


Figure 2. SEM images showing morphologies and sizes of two as-synthesized SSZ-42 samples studied here: a) single crystal (ca. 15 × 15 × 35 μm); b) powder (ca. 1–2 μm).

and  $R_{\text{Bragg}} = 0.061$  with  $\chi^2 = 1.02$ . The Rietveld difference plot in Figure 4 shows that the observed and calculated powder patterns of the calcined sample agree very well. The atomic coordinates and selected bond lengths and angles for the calcined form are listed in Tables 3 and 4, respectively.

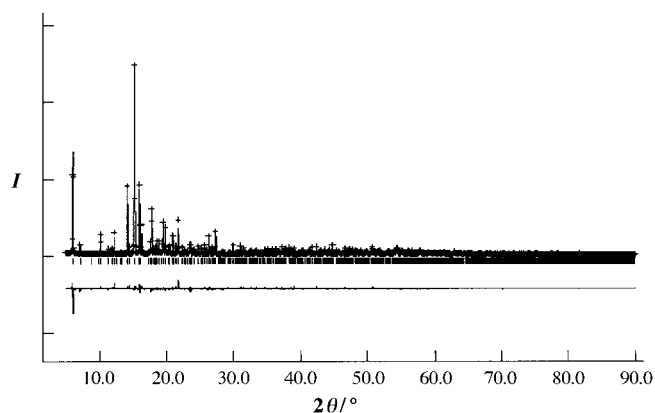


Figure 4. Results of Rietveld refinement of calcined SSZ-42 powder sample.

Table 3. Atomic coordinates and isotropic temperature parameter  $U_{\text{iso}}$  for calcined SSZ-42.

	x	y	z	$100 \cdot U_{\text{iso}} [\text{\AA}^2]$
Si1	0.9876(3)	0.6151(4)	0.6972(7)	2.6(2)
Si2	0.1471(3)	0.6159(4)	0.9006(7)	3.0(2)
Si3	0.7516(3)	0.6122(4)	0.3779(8)	2.9(2)
Si4	0.8393(3)	0.7045(4)	0.7280(8)	3.2(2)
O1	0.0625(8)	0.6427(7)	0.8284(15)	3.9(4)
O2	0.9241(6)	0.6860(7)	0.7350(13)	1.9(3)
O3	0.1769(6)	0.6785(7)	0.0793(14)	2.6(4)
O4	0	0.6250(14)	0.5	6.5(7)
O5	0.7902(6)	0.6327(8)	0.5818(16)	4.1(4)
O6	0.1944(6)	0.6372(9)	0.7491(15)	6.3(5)
O7	0.9689(8)	0.5	0.7246(21)	4.1(6)
O8	0.6801(5)	0.6819(7)	0.3206(14)	2.1(3)
O9	0.1561(7)	0.5	0.9579(21)	5.8(7)
O10	0.7219(7)	0.5	0.3540(18)	2.8(5)

Table 4. Selected bond lengths [ $\text{\AA}$ ] and angles [ $^\circ$ ] for calcined SSZ-42.

Si1–O1	1.582(8)	Si3–O5	1.595(9)
Si1–O2	1.583(8)	Si3–O6	1.554(9)
Si1–O4	1.562(4)	Si3–O8	1.606(7)
Si1–O7	1.606(5)	Si3–O10	1.599(5)
mean Si1–O	1.583	mean Si3–O	1.588
Si2–O1	1.593(8)	Si4–O2	1.576(8)
Si2–O3	1.597(8)	Si4–O3	1.587(8)
Si2–O6	1.602(9)	Si4–O5	1.604(8)
Si2–O9	1.614(4)	Si4–O8	1.590(7)
mean Si2–O	1.602	mean Si4–O	1.589
Si1–O1–Si2	147.1(5)	Si2–O6–Si3	156.1(7)
Si1–O2–Si4	149.1(6)	Si1–O7–Si1	148.2(9)
Si2–O3–Si4	143.0(6)	Si3–O8–Si4	139.2(5)
Si1–O4–Si1	170.3(13)	Si2–O9–Si3	148.6(9)
Si3–O5–Si4	148.7(6)	Si3–O10–Si3	140.2(7)

The framework structure, viewed along the 12-membered T-atom ring (12-MR) channel (Figure 5), is characterized by an undulating, one-dimensional channel system with pores comprised of 12 T-atoms. The basic building unit can be

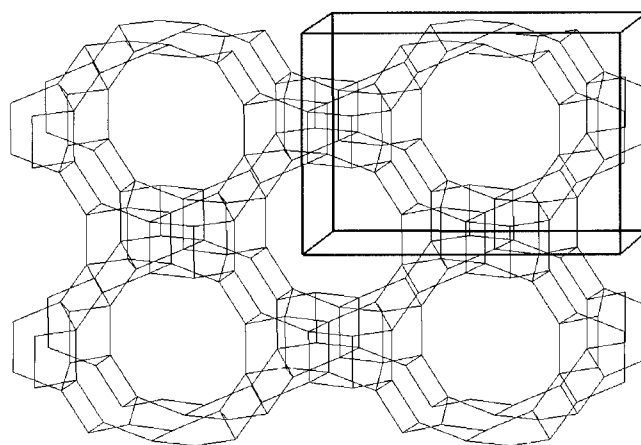


Figure 5. SSZ-42 framework viewed along [001].

considered to be a polyhedron containing 16 T-atoms which form five 4-MR, four 5-MR and two 6-MR (Figure 6). Each unit cell consists of two polyhedrons and contains, therefore,

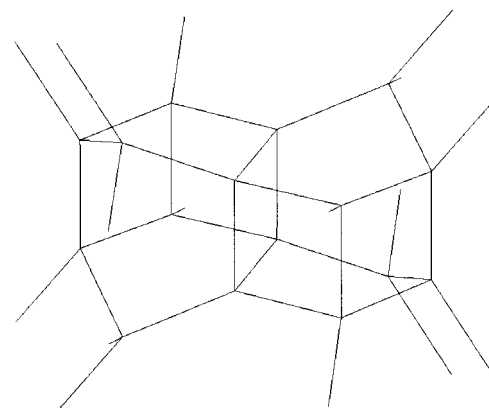


Figure 6. Basic building unit of SSZ-42 structure.

32 T-atoms. The framework density is 17.4 T per 1000  $\text{\AA}^3$ . The pore diameter at the narrowest point in the  $xz$  projection is about 6.4  $\text{\AA}$ . The cage at the widest point is about 10  $\text{\AA}$ . As shown by the  $xz$  projection in Figure 7, the channel exhibits side pockets which are reminiscent of those in beta<sup>[4]</sup> and SSZ-33<sup>[7]</sup> zeolites formed by the intersection of channels. In SSZ-42, however, there are no intersecting channels. In the perpendicular projection ( $yz$ ) there are no undulations and the pore diameter is about 6.7  $\text{\AA}$ . An  $xy$  projection of the unit cell is shown in Figure 8. As demonstrated by the numbered T-atoms in Figure 8, it is clear that the 12-MR is considerably distorted, giving the smaller than expected pore size. At first glance it appears to be a 10-MR (vide infra). The propensity for a high 4-MR population in a high-silica zeolite structure, in relation to the necessity for lattice substitution (boron for silicon, in this instance), has been discussed by Zones and Santilli.<sup>[39]</sup>

Additionally, Cambor et al. have very recently reported the structure determination of the pure-silica zeolite ITQ-4.<sup>[40]</sup> Their reported structure for the pure-silica ITQ-4 and our structure solution for the borosilicate SSZ-42 are in very good agreement.

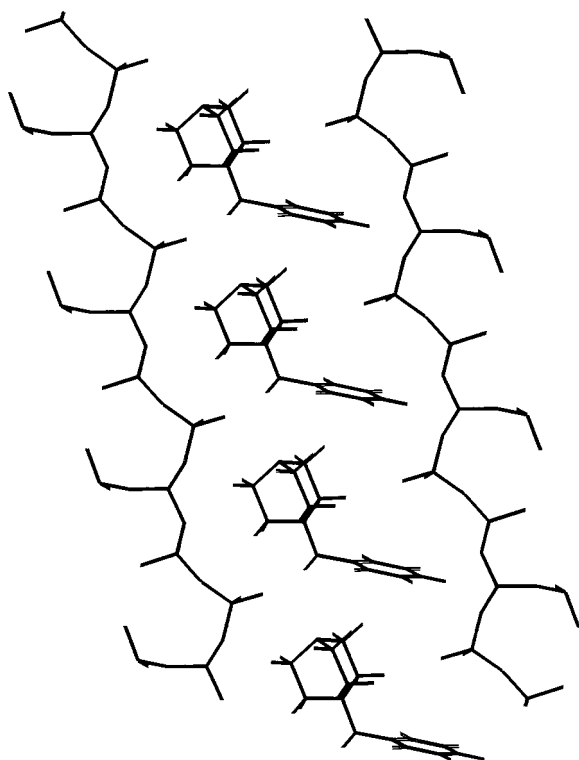


Figure 7. *xz* projection of SSZ-42 framework showing minimized location of template molecules.

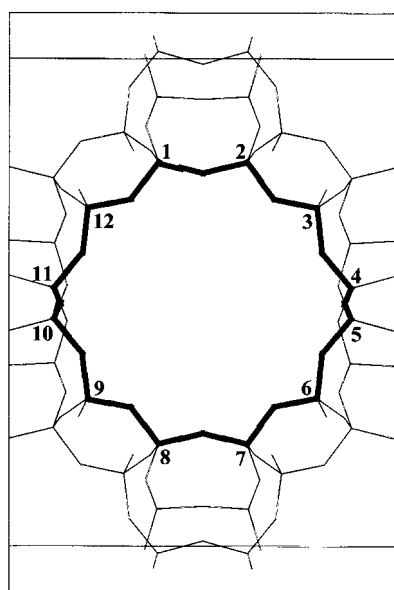


Figure 8. *xy* projection of the unit cell and 12-MR pore of SSZ-42.

**Computer modeling:** The powder diffraction data from the as-synthesized sample, which still contains the template used in synthesis, displays considerable electron density in the channel. The diffraction pattern displays only diffraction maxima consistent with a C-centered lattice; therefore, the template molecules must be disordered for space group  $C2/m$ . Results from elemental analyses indicate two template molecules per unit cell. A possible location for the template molecules was generated by molecular modeling in the Insight computational environment<sup>[41]</sup> (see Figure 7). The template

molecule spans the volume from one side pocket diagonally to the next. The stabilization energy (SE) was  $-263.8$  kcal per template molecule calculated with a single template molecule in the pore. With four templates packed in a pore channel, four unit cell repeats in length, the SE was  $-123.1$  kcal per template molecule. The reduction in SE with four template molecules is due to template–template interactions. If the template molecules had long-range ordering in the channels, the symmetry would be reduced relative to that of the framework. The extra peaks corresponding to this reduction are not observed; therefore, we assume that the template molecules are disordered. Because the symmetry of the framework would result in four equivalent positions for the molecules, we assume that each has  $1/4$  occupancy. The difference electron density in the channels is reduced by this model; however, there are still considerable discrepancies in the calculated structure factors. Figure 7 shows templates in a head to tail orientation. Rotation of a template molecule about the twofold axis at  $1/2, y, 1/2$  results in equivalent orientations with respect to the framework but with head to head and tail to tail orientations with respect to other templates. Modeling suggests that these all have similar energies. Because the template molecule has lower symmetry than the framework, these equivalent orientations could result in considerable disorder for the Rietveld structural model. Further studies on the structure refinement based on the as-synthesized synchrotron powder XRD pattern are in progress.

This structure confirms once again the effective use of organo cations as guest molecules in developing the host molecular sieve architecture. The fact that the relatively linear guest molecule does not reside parallel to the pore in this structure is a relatively unusual occurrence in zeolite crystallization. Rather, the molecule resides in a sequence of bulging cages formed at a fixed off-pore axis direction from the main channel.

**$^{13}\text{C}$  MAS NMR spectroscopy:** The  $^{13}\text{C}$  MAS NMR spectra are shown in Figure 9 for as-synthesized SSZ-42 powder sample. The spectral assignments of the intact template molecules are shown in the spectrum in Figure 9a.<sup>[42]</sup> The mobility of the template molecule occluded inside the zeolite was investigated by dipolar-dephasing (DD).<sup>[26, 27]</sup> This experiment detects the coherent magnetization after a brief period without high-power proton decoupling. Parts of the molecule that experience rapid molecular reorientation (with respect to the magnetic field) that effectively average the heteronuclear dipolar coupling still appear in the NMR spectrum. The resonances that arise from more rigid parts of the molecule will not be able to average the strong dipolar coupling and will become dephased, that is, absent in the NMR spectrum. The result of the DD experiment for the template molecules occluded in SSZ-42 is shown in the spectrum in Figure 9b. The methylene resonance 3 and resonances 5, 6 from the phenyl ring are absent from the spectrum, indicating that this end of the template molecule is not undergoing molecular reorientation (faster than  $10^3$  s). The difference spectrum (Figure 9c) is also shown for clarity. The methylene carbon atoms in the DABCO end of the template molecule undergo significant

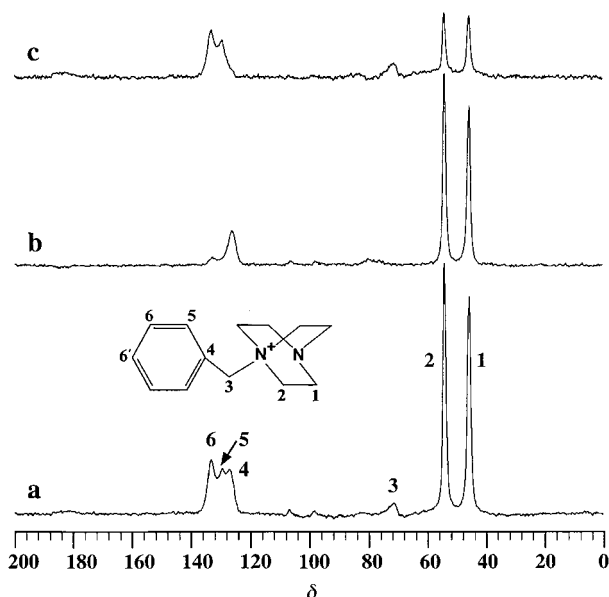


Figure 9. a)  $^{13}\text{C}$  CP/MAS NMR spectrum of as-synthesized SSZ-42 powder sample; spinning sidebands have been suppressed with the TOSS pulse sequence. The C6 and C6' resonances overlap in this spectrum. b) The dipolar-dephasing spectrum is shown for the same sample;  $^1\text{H}$ -decoupling was turned off during the first delay of the TOSS sequence, 28.5  $\mu\text{sec}$ . c) The difference between spectra a and b is shown; the spectral intensity represents the fraction of magnetization that dephased without proton-decoupling.

molecular reorientation on the ms time-scale, which is most likely a twisting motion about the  $\text{C}_2$  axis. This is evident since the majority of the  $^{13}\text{C}$  spectral intensity survives the dipolar-dephasing period (Figure b). Resonance 4, the quaternary carbon of the phenyl ring, also survives the DD experiment, because it has no directly bonded protons. Variable contact time cross-polarization (CP) experiments (not shown) show a weak  $^1\text{H}$ - $^{13}\text{C}$  dipolar coupling consistent with the major source of CP magnetization being the mobile DABCO protons. The  $^{13}\text{C}$  CP/MAS NMR results supports the picture (from single-crystal X-ray and computer simulations) that the template molecules are oriented with respect to the zeolite channel system. The lack of rapid molecular reorientation for the benzyl end of the template molecule also implies that there is a tight fit between the organic molecule and the zeolite framework, as also evidenced by the results discussed above (see Table 1).

**HREM:** Eleven distinct selected area zone axis electron diffraction patterns were collected from approximately 15 different crystals. Figure 10 shows two diffraction patterns later identified as the [100] (left) and [001] (right) orientations. We were able to index all the electron diffraction patterns by using

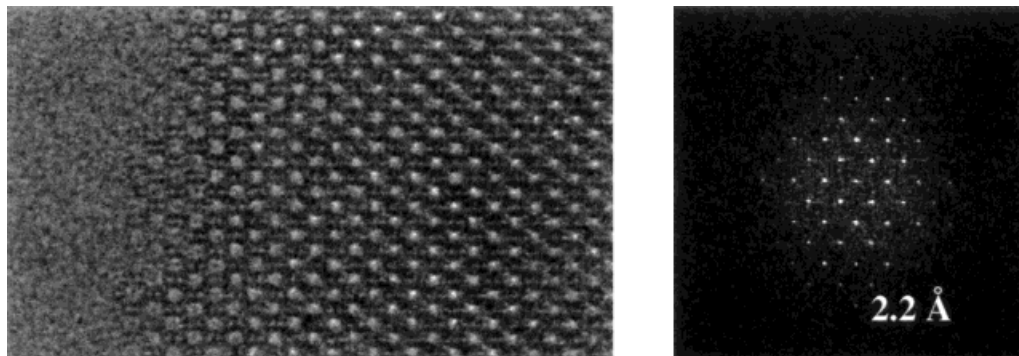


Figure 11. Left: Low-dose high resolution image from SSZ-42 crystal in [001] orientation. The image was recorded from a wedge-shaped crystal resulting in a gradation of the image intensity from left to right. Right: Digital diffractogram of Figure 11 left showing information out to 2.2 Å.

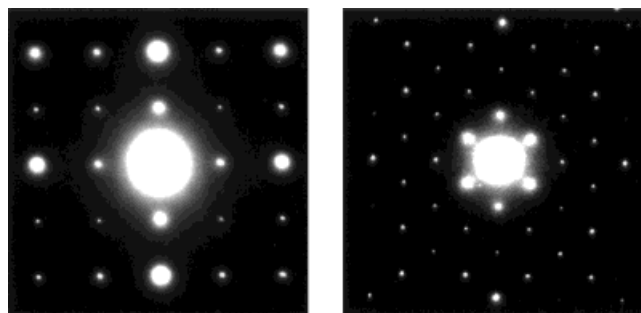


Figure 10. Electron diffraction patterns from small crystals of SSZ-42 in [100] (left) and [001] orientations (right), respectively.

the unit cell model constructed from the X-ray diffraction data. All the diffraction spots in the electron diffraction patterns were sharp. No streaking was observed in any of the orientations. This indicates that there are no stacking faults in SSZ-42 and suggests that only one polymorph of the material is present.

A low-dose HREM image recorded from a wedge-shaped crystal in the [001] projection is shown in Figure 11 left. The characteristic large white dot contrast shows that a main channel runs along the [001] direction in the crystal. The digital diffractogram from this image (Figure 11 right) shows that the image, though noisy, contained information out to at least 2.2 Å. Figure 12 left is a processed unit cell motif obtained by applying real space noise reduction techniques of Pan and Crozier<sup>[43]</sup> to Figure 11 left. Initial measurements from the processed image suggested that the channel circumference was approximately 29 Å. Assuming that the Si–O bond length and angles are in the range of 1.55–1.64 Å and 140–170°, respectively, a 10-MR of Si atoms has a circumference of 29–32 Å. This initial analysis led us to the preliminary proposal that the main channel shown in Figure 12 left may correspond to the projection of an untilted 10-MR running along the [001] direction; however, we were unable to come up with a structure that would yield a good fit between the simulated and experimental image. Although, if we use the atomic coordinates derived from the XRD data, we obtain an excellent match between the simulated and experimental HREM data (see Figure 12 middle).

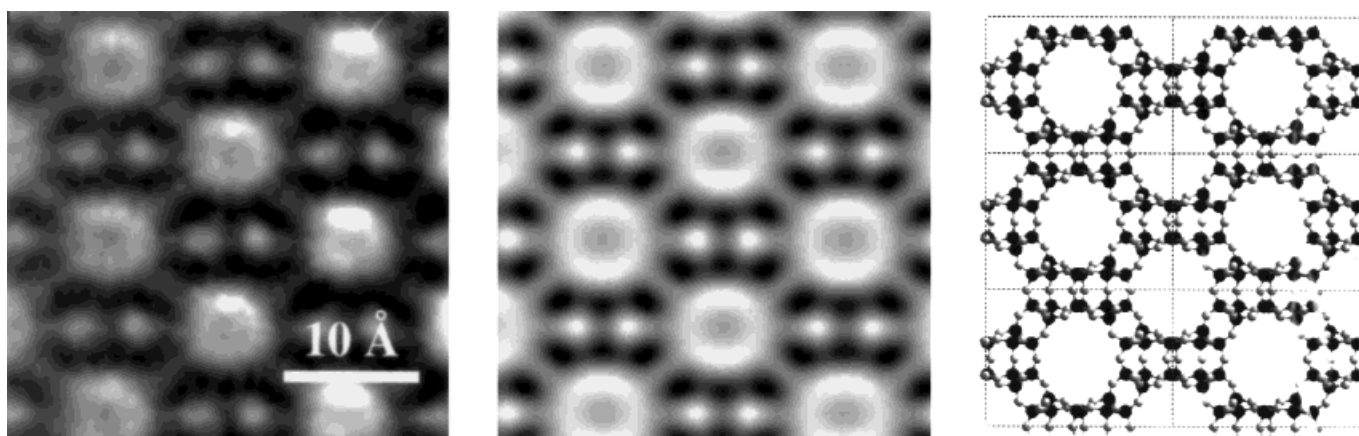


Figure 12. Left: Spatially averaged imaged motif generated from Figure 11 left showing structure information in zeolite unit cells. Middle: Simulated image of the determined SSZ-42 structure in the [001] projection. The image was calculated using multislice techniques for a crystal 40 Å in thickness and the objective lens set to Scherzer defocus (−490 Å). Right: Projection of the determined structure along the [001] direction.

Low-dose high-resolution electron microscopy (HREM) has proven to be a useful technique for elucidating the structure of zeolites, as demonstrated for SSZ-33,<sup>[7]</sup> VPI-8,<sup>[11]</sup> and SSZ-31.<sup>[13]</sup> In those cases, HREM helped in providing the first guess of the structure model and later took on the role of a stringent test in verifying the eventual model. In the current case of SSZ-42, the unusual nature of the undulating channel causes the 12-MR to appear as a 10-MR ring in [001] projection (see Figure 12 right). This points out that great care must be exercised when interpreting data from HREM in terms of crystal structural units. Nonetheless, the comparison between the experimental and simulated images is still clearly a stringent test of the accuracy of the proposed structure model.

**Physisorption:** Table 5 lists the zeolites studied in this work for argon adsorption, together with their pore size and dimensionality. SSZ-42 was compared with 1) SSZ-26/SSZ-33 and beta (multidimensional 10/12- or 12/12-MR channel

Table 5. Zeolites studied in this work for argon adsorption and their pore structures.

Zeolite	Pore structure
SSZ-42	1D undulating channel, distorted 12-MR
SSZ-26/SSZ-33	3D channel, 10-/12-/12-MR
Beta	3D channel, 12-MR
SSZ-24	1D straight channel, 12-MR
SSZ-31	1D straight channel, 12-MR
ZSM-12	1D straight channel, distorted 12-MR
L	1D straight channel 12-MR, with small side pocket
EU-1	1D, 10-MR, with side pocket
SSZ-25	2D, 10-MR, with cage
SSZ-37	2D, 10-MR, with cage
SSZ-32	1D straight channel, 10-MR

system), 2) SSZ-24, SSZ-31, ZSM-12 and L (one-dimensional 12-MR channel system), 3) EU-1, SSZ-25 and SSZ-37 (10-MR channel system with side pocket/cage), and 4) SSZ-32 (one-dimensional 10-MR channel system). The adsorption results are depicted in Figure 13. Argon adsorbed in the micropores of SSZ-42 over a broad pressure range, from about 10 μbar to

about 1000 μbar, even during static experiments with adequate time for equilibration. Equilibrium micropore-filling steps for most other zeolites occurred over much narrower ranges. The only other zeolites that we have found to have such broad micropore-filling transitions are SSZ-26, SSZ-33, and beta (Figure 13). Adsorption isotherms for SSZ-42 and SSZ-26 are very close to one another in the micropore-filling region (Figure 14), although they diverge at higher pressures due to a large external surface area for SSZ-26. The micropore volume accessible to argon in SSZ-42 is 0.20 mL g<sup>−1</sup>, about 10% lower than that for SSZ-26. Its external area is about 10 m<sup>2</sup> g<sup>−1</sup>. Detailed discussion on the above argon adsorption results will be reported later.

The existence of large pores in SSZ-42 was also experimentally confirmed by the adsorption of a series of molecules with varying dimensions. Fast adsorption was observed with both 1,2,4- and 1,3,5-triisopropylbenzene (larger than the 1,2,4-isomer) in zeolite UTD-1 (10 Å pore) as well as with 1,2,4-triisopropylbenzene in zeolite Y (7.3 Å pore), while the adsorption of 1,3,5-triisopropylbenzene in zeolite Y proceeded extremely slowly.<sup>[44]</sup> Within the experimental errors, no uptake of 1,3,5-triisopropylbenzene in SSZ-42 was detected. However, the adsorption capacity of SSZ-42 for the less bulky 1,2,4-triisopropylbenzene reached about 0.07 mL g<sup>−1</sup> after five days, indicating a strongly hindered diffusion of this molecule through the distorted 12-MR openings. Similar to argon adsorption, all smaller adsorbates screened such as N<sub>2</sub>, *n*-hexane, 2,2-dimethylbutane, and cyclohexane had a high adsorption capacity of about 0.20 mL g<sup>−1</sup> in SSZ-42, which is close to the adsorption data obtained in SSZ-33 and beta, both of which possess intersecting 10/12- or 12/12-MR channels. Based on the above results from argon, nitrogen, and hydrocarbon adsorption, one could easily come to the incorrect conclusion that the framework architecture of this new material consists of an intersecting 10/12- or 12/12-MR channel system. In fact, the large adsorption capacity of SSZ-42 is due to large cages rather than to an intersecting channel system. The high adsorption capacity exhibited here is exceptional for a large-pore zeolite with a one-dimensional channel system. This is the first reported zeolite structure with such features.



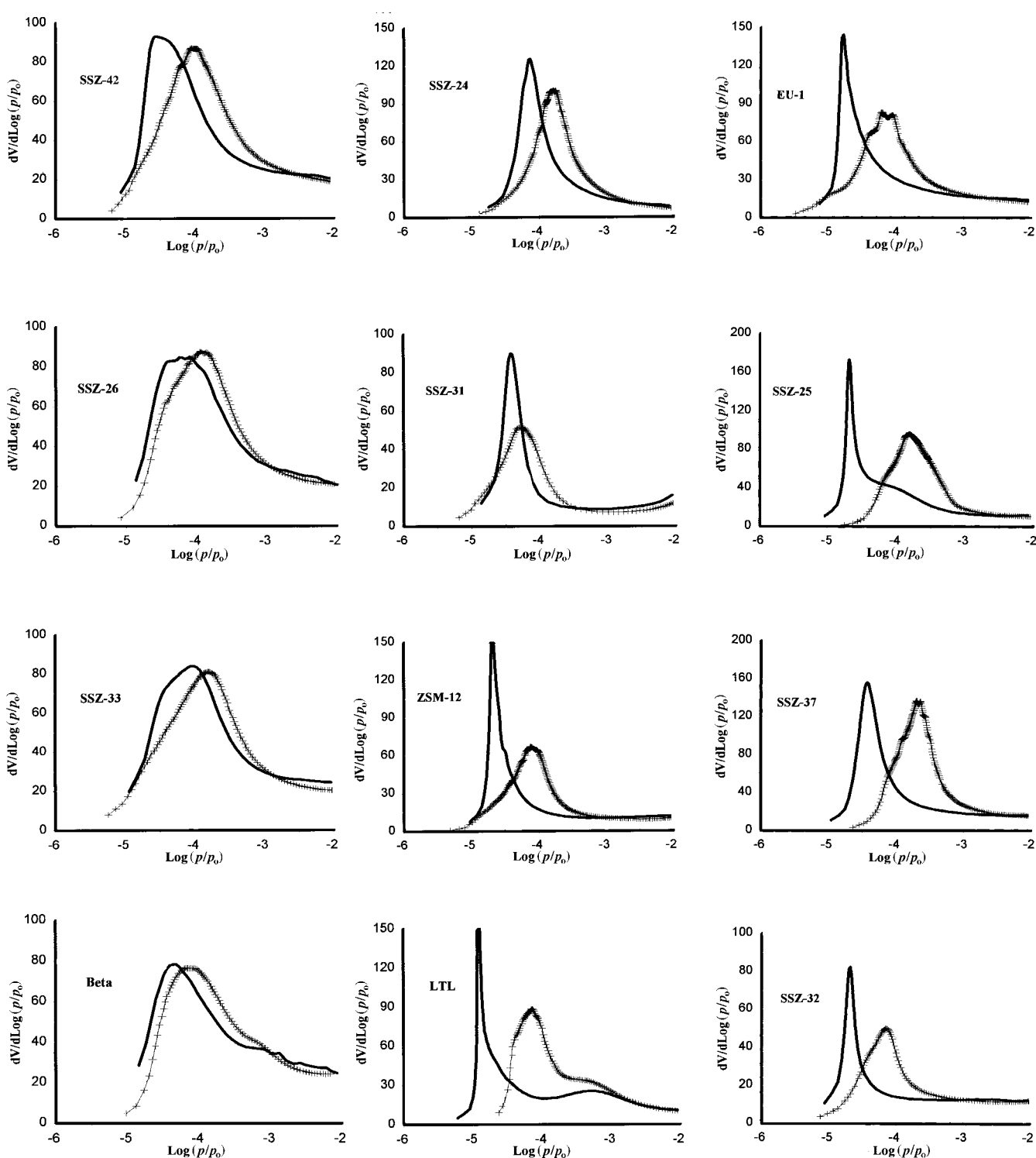


Figure 13. Derivatives of argon physisorption isotherms for various zeolites. Solid lines: static measurements; + : dynamic measurements.

**Additional physicochemical characterization:** The IR spectrum of SSZ-42 (Figure 15) in the  $350\text{ cm}^{-1}$  to  $1700\text{ cm}^{-1}$  region was unique among the spectra of 150 zeolite and zeolite-like materials that we have tested. The closest match among our other zeolite spectra was that of SSZ-26.

**Catalysis:** SSZ-42 is very stable up to at least  $800^\circ\text{C}$  even under hydrothermal conditions. By manipulation of synthesis

conditions, it can be prepared with a wide range of Brønsted acidity and, therefore, can be converted to different catalysts for a body of chemical reactions, including hydrocracking, catalytic cracking, isomerization, alkylation of aromatic compounds, and reforming. In the light of its unusual topological structure and exceptional pore volume, this new material exhibits many interesting catalytic characteristics and, as we reported previously,<sup>[15, 16]</sup> generates a series of catalysts for several industrial processes.

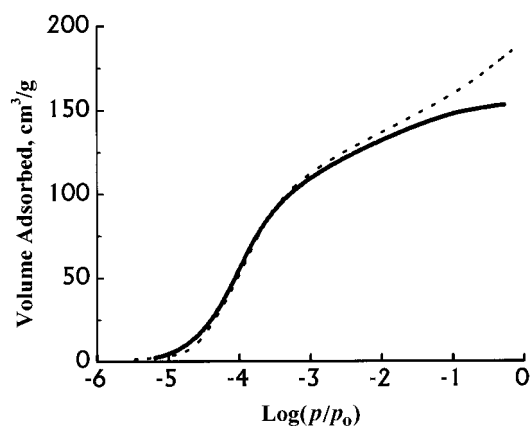


Figure 14. Argon physisorption isotherms for SSZ-42 (solid line) and SSZ-26 (dotted line). Continuous flow measurements at  $-186^{\circ}\text{C}$  with a dosing rate that filled the micropores in one and one-half hours.

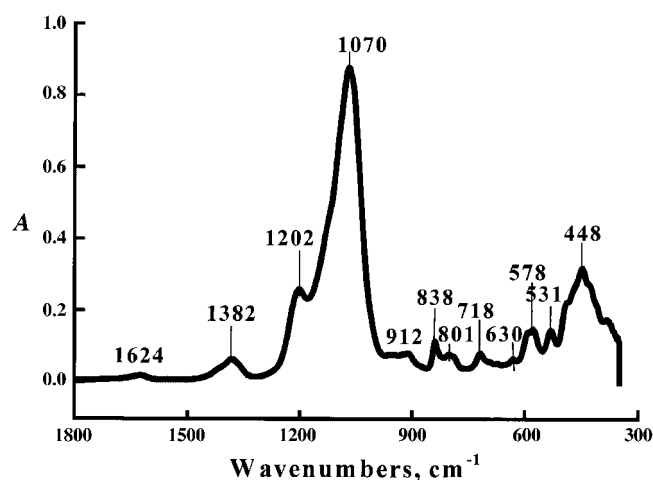


Figure 15. IR spectrum of calcined SSZ-42 obtained with a diamond ATR cell.

An aluminum-containing SSZ-42 sample was prepared by substituting aluminum for most of the boron in B-SSZ-42 by using aqueous aluminum nitrate solution<sup>[16]</sup> and was characterized by the constraint index (CI). The CI is widely used to characterize the effective pore size of acidic zeolites and is determined based on a comparison of the rates of acid-catalyzed cracking of *n*-hexane and 3-methylpentane with an equimolar mixture of these two hydrocarbons as feed.<sup>[28]</sup> The Al-SSZ-42 sample studied here had a CI value of 0.65 which is typical of the 12-MR (or larger pore) zeolites.

Al-SSZ-42 was also studied for ethylbenzene disproportionation. This reaction was used as a test reaction for the rapid discrimination between 12- and 10-MR zeolites.<sup>[29]</sup> According to Weitkamp et al., an induction period is characteristic of the 12-MR zeolites (e.g., Y and ZSM-12), namely, the ethylbenzene conversion increases with the time-on-stream at the onset of the reaction. It is followed by a stationary or quasi-stationary stage during which the conversion remains constant or decreases slowly. With 10-MR zeolites, there is no induction period and the catalyst deactivation is considerably faster. Pronounced differences are encountered between the distributions of the diethylbenzene isomers formed on 12- and 10-MR zeolites: 1) with 12-MR zeolites, in the quasi-stationary stage the isomer distributions are essentially inde-

pendent of the time-on-stream and close to the thermodynamic equilibrium; 2) with 10-MR zeolites, the selectivity for 1,2-diethylbenzene is very low and the isomer distributions change significantly with the time-on-stream in favor of the *para*-selectivity (1,4-diethylbenzene). In addition, the difference between the yields (Y) of benzene and diethylbenzenes is also pronounced although equal molar yields of benzene and diethylbenzenes are expected based on stoichiometry: on 12-MR zeolites, the molar ratio of  $Y_{\text{DE-Bz}}/Y_{\text{Bz}}$  typically amounts to 0.9 as compared to 0.75 on 10-MR zeolites.

The time-on-stream behavior of SSZ-42 during ethylbenzene disproportionation is depicted in Figure 16. No induction

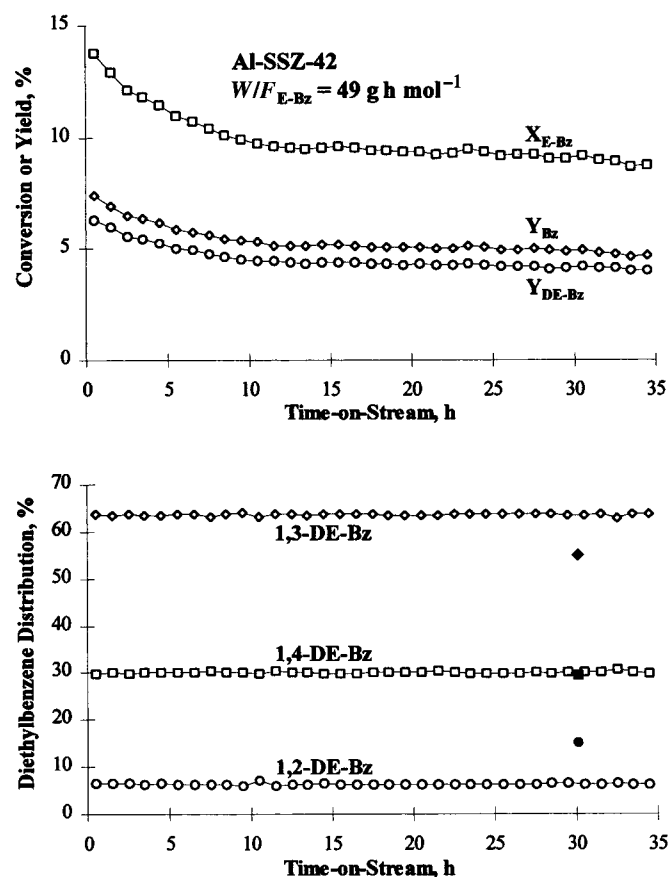


Figure 16. Top: Conversion of ethylbenzene ( $X_{\text{E-Bz}}$ ) and yields of benzene ( $Y_{\text{Bz}}$ ) and diethylbenzenes ( $Y_{\text{DE-Bz}}$ ) over SSZ-42. Bottom: Distributions of the diethylbenzene isomers over SSZ-42. The full symbols (single points) represent calculated values for the thermodynamic equilibrium at  $250^{\circ}\text{C}$ .<sup>[29]</sup>  $W/F_{\text{E-Bz}}$  stands for the modified residence time, where  $W$  is the mass of the dry catalyst and  $F_{\text{E-Bz}}$  is the molar flux of ethylbenzene at the reactor inlet.

period was observed and the deactivation was considerable, implying that SSZ-42 appears to be a 10-MR zeolite. However, the molar  $Y_{\text{DE-Bz}}/Y_{\text{Bz}}$  ratio was close to 0.9, which suggests, together with the distributions of the diethylbenzene isomers shown in Figure 16 bottom, that SSZ-42 is a 12-MR zeolite. This less straightforward picture obtained from SSZ-42 is most likely related to the unusual framework structure of this novel zeolite. Further work is in progress in our laboratory with SSZ-26/SSZ-33, beta, L, and other zeolites to investigate the relationships between their structures and catalytic behaviors in ethylbenzene disproportionation.

Furthermore, the Al-SSZ-42 material was loaded with 0.27 wt. % Pd and the resulting Pd/Al-SSZ-42 was characterized by using the Spaciousness Index (SI). The SI is defined as the yield ratio of isobutane and *n*-butane in hydrocracking of a C<sub>10</sub> cycloalkane such as *n*-butylcyclohexane over bifunctional zeolites or other molecular sieve materials.<sup>[30, 31]</sup> The ratio increases with increasing pore size and is proven to be a useful tool for characterizing the shape-selective properties of molecular sieve materials. Based on our results, SSZ-42 has an SI of 15. In Figure 17, the SI of SSZ-42 is compared to those of various reported zeolites. According to the above results,

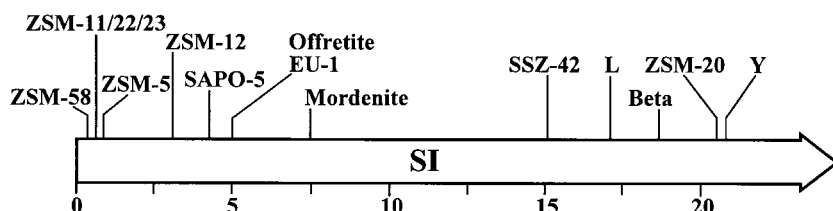


Figure 17. The Spaciousness Indices of SSZ-42 and selected molecular sieves.

the effective void size of SSZ-42 is smaller than the effective diameter of the largest voids in Y, ZSM-20, beta, and L but larger than those of other one-dimensional 12-MR zeolites. Apparently, the SI data are consistent with the SSZ-42 structure discussed in this study.

## Conclusion

This paper describes the discovery, synthesis, structure determination, physicochemical and catalytic characterization of the novel zeolite SSZ-42. This material could well be suitable for commercial applications because it is stable up to at least 800 °C under thermal and hydrothermal conditions. Preliminary testing showed that it exhibits many interesting characteristics concerning a body of chemical reactions and promises to be a useful catalyst for hydrocarbon processing.

The crystalline architecture of SSZ-42 is characterized by an undulating, one-dimensional 12-MR channel system. This configuration is a surprise given that the measured adsorption capacity is much higher than expected for a one-dimensional system and that the early HREM results suggested it was a one-dimensional 10-MR system. This work clearly points out the importance of using a collaborative multitechnique, interdisciplinary approach for the structural solution.

**Acknowledgements:** We thank Chevron Research and Technology Company for support of zeolite research in the catalyst area, especially D. J. O'Rear, S. A. Bezman, and C. M. Detz. The high-resolution powder diffraction data were obtained, with the assistance of D. E. Cox and Q. Zhu, at the National Synchrotron Light Source, Brookhaven National Laboratory, which is supported by the U. S. Department of Energy, Division of Materials Sciences and Division of Chemical Sciences. We thank G. Zhang and G. S. Mondo for assistance in taking the XRD data, and L. T. Yuen and T. F. Finger for technical assistance in synthesis and catalysis. We thank M. Pan of Gatan, Inc. for useful comments on the HREM images. P.A.C. was supported by the Industrial Associates Program at Arizona State University and made use of the Center for HREM supported by NSF Grant DMR-91-15680.

- [1] S. I. Zones, M. E. Davis, *Curr. Opin. Solid State Mater. Sci.* **1996**, *1*, 107.
- [2] C. Baerlocher, L. B. McCusker, *Stud. Surf. Sci. Catal.* **1994**, *85*, 391.
- [3] N. A. Briscoe, D. W. Johnson, M. D. Shannon, G. T. Kokotailo, L. B. McCusker, *Zeolites* **1988**, *8*, 74.
- [4] J. M. Newsam, M. M. J. Treacy, W. T. Koetsier, C. B. deGruyter, *Proc. Roy. Soc. Lond. A* **1988**, *420*, 375.
- [5] S. L. Lawton, W. J. Rohrbaugh, *Science* **1990**, *247*, 1319.
- [6] M. D. Shannon, J. L. Casci, P. A. Cox, S. J. Andrew, *Nature* **1991**, *353*, 417.
- [7] R. F. Lobo, M. Pan, I. Y. Chan, H. X. Li, R. C. Medrud, S. I. Zones, P. A. Crozier, M. E. Davis, *Science* **1993**, *262*, 1543.
- [8] M. E. Leonowicz, J. A. Lawton, S. L. Lawton, M. K. Rubin, *Science* **1994**, *264*, 1910.
- [9] B. Marler, A. Grünwald-Lücke, H. Gies, *Zeolites* **1995**, *15*, 388.
- [10] C. C. Freyhardt, M. Tsapatsis, R. F. Lobo, K. J. Balkus, Jr., M. E. Davis, *Nature* **1996**, *381*, 295.
- [11] C. C. Freyhardt, R. F. Lobo, S. Khodabandeh, J. E. Lewis, Jr., M. Tsapatsis, M. Yoshikawa, M. A. Cambor, M. Pan, M. M. Helmkamp, S. I. Zones, M. E. Davis, *J. Am. Chem. Soc.* **1996**, *118*, 7299.
- [12] L. B. McCusker, R. W. Grosse-Kunstleve, C. Baerlocher, M. Yoshikawa, M. E. Davis, *Microporous Mater.* **1996**, *6*, 295.
- [13] R. F. Lobo, M. Tsapatsis, C. C. Freyhardt, I. Y. Chan, C. Y. Chen, S. I. Zones, M. E. Davis, *J. Am. Chem. Soc.* **1997**, *119*, 3732.
- [14] C. Y. Chen, L. W. Finger, R. C. Medrud, P. A. Crozier, I. Y. Chan, T. V. Harris, S. I. Zones, *Chem. Commun.* **1997**, 1775.
- [15] C. Y. Chen, A. Rainis, S. I. Zones, in *Advanced Catalytic Materials - 1996*, *Mat. Res. Soc. Symp. Proc. Vol. 454*, (Eds.: P. W. Lednor, M. J. Ledoux, D. A. Nagaki, L. T. Thompson), Materials Research Society, **1997**, 205.
- [16] S. I. Zones, A. Rainis, *WOP 95/908793*, **1995**.
- [17] SHELXTL, Version 5.03. We acknowledge the help of the Applications Laboratory of Siemens Energy and Automation, Inc., Madison, WI, USA, in the collection of intensity data for the single crystal.
- [18] D. E. Cox, J. B. Hastings, L. P. Cardoso, L. W. Finger, *Mat. Science Forum* **1986**, *9*, 1.
- [19] A. Le Bail, H. Duray, J. L. Fourquet, *Mat. Res. Bull.* **1988**, *23*, 447.
- [20] D. E. Cox, personal communication to L. W. Finger, **1996**.
- [21] L. W. Finger, D. E. Cox, A. P. Jephcoat, *J. Appl. Cryst.* **1994**, *27*, 892.
- [22] A. C. Larson, R. B. Von Dreele, *GSAS - General Structure Analysis System*, Los Alamos National Laboratory Report LA-UR 86-748, **1986**.
- [23] S. C. Abrahams, E. T. Keve, *Acta Cryst. A* **1971**, *27*, 157.
- [24] N. C. Popa, *J. Appl. Cryst.* **1992**, *25*, 611.
- [25] C. Y. Chen, S. I. Zones, unpublished results.
- [26] D. P. Raleigh, E. T. Olejniczak, S. Vega, R. G. Griffin, *J. Magn. Reson.* **1987**, *72*, 238.
- [27] S. J. Opella, M. H. Frey, *J. Am. Chem. Soc.* **1979**, *101*, 5894.
- [28] V. J. Frilette, W. O. Haag, R. M. Lago, *J. Catal.* **1981**, *67*, 218.
- [29] J. Weitkamp, S. Ernst, P. A. Jabobs, H. G. Karge, *Erdöl und Kohle-Erdgas* **1986**, *39*, 13.
- [30] J. Weitkamp, S. Ernst, R. Kumar, *Appl. Catal.* **1986**, *27*, 207.
- [31] J. Weitkamp, S. Ernst, C. Y. Chen, in *Zeolites: Facts, Figures, Future, Proc. 8th Int. Zeolite Conf., Studies in Surface Science and Catalysis 49*, (Eds.: P. A. Jacobs, R. A. van Santen) Elsevier, **1989**, 1115.
- [32] S. I. Zones, *US Patent 4,508,837*, **1985**.
- [33] R. F. Lobo, S. I. Zones, R. C. Medrud, *Chem. Mater.* **1996**, *8*, 2409.
- [34] S. I. Zones, Y. Nakagawa, L. T. Yuen, T. V. Harris, *J. Am. Chem. Soc.* **1996**, *118*, 7558.
- [35] S. I. Zones, L. T. Yuen, Y. Nakagawa, R. A. Van Nordstrand, S. D. Toto, in *Proc. 9th. Int. Zeolite Conf.*, (Eds.: R. von Ballmoos, J. B. Higgins, M. M. J. Treacy), Butterworth-Heinemann, **1993**, 163.
- [36] S. I. Zones, Y. Nakagawa, *Microporous Mater.* **1994**, *2*, 543.
- [37] E. W. Valyocsik, *US Patent 5,441,721*, **1995**.
- [38] M. A. Cambor, A. Corma, L. A. Villaescusa, *Chem. Commun.* **1997**, 749.

- [39] S. I. Zones, D. S. Santilli, in *Proc. 9th. Int. Zeolite Conf.*, (Eds.: R. von Ballmoos, J. B. Higgins, M. M. J. Treacy), Butterworth–Heinemann, **1993**, 171.
- [40] P. A. Barrett, M. A. Cambor, A. Corma, R. H. Jones, L. A. Villaescusa, *Chem. Mater.* **1997**, *9*, 1713.
- [41] Template docking studies were done with the CVFF forcefield using Solids-Docking and Discover modules of computer software distributed by the Catalysis and Sorption Consortium of Molecular Simulations, Inc., San Diego, CA.
- [42] Spectral assignments agree with spectra and multiplicities given for other benzyl quaternary ammonium molecules in *The Aldrich Library of <sup>13</sup>C and <sup>1</sup>H FT NMR Spectra*, (Eds.: C. J. Pouchert, J. Behnke), Aldrich, **1993**.
- [43] M. Pan, P. A. Crozier, *Ultramicroscopy* **1993**, *48*, 332.
- [44] R. F. Lobo, M. Tsapatsis, C. C. Freyhardt, S. Khodabandeh, P. Wagner, C. Y. Chen, K. J. Balkus, Jr., S. I. Zones, M. E. Davis, *J. Am. Chem. Soc.* **1997**, *119*, 8474.
-